Jpn. J. Appl. Phys. Vol. 33 (1994) pp. L 1316–L 1319
Part 2, No. 9B, 15 September 1994

Electron Energy-Loss Spectra of Single-Shell Carbon Nanotubes

Ryuichi KUZUO*, Masami TERAUCHI, Michiyoshi TANAKA and Yahachi SAITO[1]

Research Institute for Scientific Measurements, Tohoku University, Sendai 980
[1] *Department of Electrical Engineering, Faculty of Engineering, Mie University, Tsu 514*

(Received June 3, 1994; accepted for publication August 20, 1994)

Transmission electron energy-loss spectra of single-shell carbon nanotubes were measured and compared with those of multishell carbon nanotubes and graphite. Two peaks due to the π plasmon and the $\pi+\sigma$ plasmon were observed at 5.8 eV and 20.6 eV, respectively. The energy of the π plasmon takes a value between those of two kinds of multishell tubes. The energy of the $\pi+\sigma$ plasmon is lower than those of multishell tubes and graphite by 2 eV and 6 eV, respectively. The 1s$\rightarrow\pi^*$ and 1s$\rightarrow\sigma^*$ transition peaks of the single-shell tubes are much broader than those of the multishell tubes and graphite. The reason for the broadening may be due to the strong curving of the graphitic sheets.

KEYWORDS: carbon nanotube, single-shell tube, fullerene, EELS, bulk plasmon, interband transition

In 1991, Iijima[1)] discovered a new type of carbon needle that can be produced by the arc-discharge evaporation method similar to that used for producing fullerenes. The carbon needles, which can be called "carbon nanotubes" or "buckytubes," have been observed by high-resolution transmission electron microscopy.[1,2)] It has been revealed that carbon nanotubes consist of 2 to 50 coaxial cylinders of graphitic sheets, and the carbon atom hexagons on a tube are arranged in a helical fashion about the needle axis. Recently, the production of carbon nanotubes consisting of a single-layer graphitic sheet was discovered. These carbon nanotubes, which are called "single-shell tubes" as opposed to multishell tubes, have been produced by arc-discharge of carbon with iron[3)] or cobalt[4)] as a catalyst. Saito and coworkers[5,6)] have succeeded in the production of single-shell tubes using nickel as a catalyst, and have reported nickel to be an effective catalyst for producing single-shell tubes.

Band structure calculations[7-12)] have shown that the electronic structures of single-shell tubes are categorized as metallic or semiconducting depending on the diameter and chirality of the tubes. In spite of a great deal of interest in their electronic properties, the measurements of their electronic properties have not yet been realized because the diameters of multishell tubes are so small as to range from a few to a few tens of nanometers. Hence, the electronic properties of carbon nanotubes have been measured only by electron energy-loss spectroscopy (EELS) with use of transmission electron microscopes (TEMs).[13-15)] We have revealed[13)] that the energies of the two peaks due to the π plasmon and the $\pi+\sigma$ plasmon of multishell tubes are different from those of graphite. Recently, Wang *et al.*[15)] reported that the spectra from single-shell tubes did not exhibit the π plasmon peak.

The present paper reports the transmission electron energy-loss spectra of single-shell tubes and the dielectric function derived by Kramers-Kronig analysis of the loss function obtained. These results are compared with those of multishell carbon nanotubes and graphite.

Single-shell tubes used in the present study were produced by the d.c. arc-discharge method using nickel as a catalyst. The details of the production of single-shell tubes are given in papers by Saito and coworkers.[5,6)] Specimens for EELS were prepared by dropping a suspension of acetone containing single-shell tubes onto a specimen-supporting copper mesh covered with a microgrid for electron microscopy.

The high-resolution electron energy-loss spectrometer used was developed as a Joint Research with Industry project by the Ministry of Education, Science and Culture.[16-18)] The spectrometer was equipped with a thermal-type field emission gun (FEG) as the electron source and specially designed double-focus Wien filters[19)] as the monochromator and the analyzer. As the illumination lens system, the specimen goniometer and the imaging lens system of the spectrometer, the column part of a JEM-1200EX was utilized. The electron energy-loss signals were received by the parallel detection system using a charge-coupled device (CCD) camera. The best values of the full widths at half-maximum (FWHM) of the zero-loss peak at present are 15 meV and 30 meV for cases without and with a specimen, respectively. The accelerating voltage of the incident electron beam was set at 60 kV. The retarding potential of the monochromator was set to be 51 V, and that of the analyzer was set to be 200–720 V. The spectra were measured from areas of 100 nmϕ in 180–240 s at room temperature. The spectra of single-shell tubes were measured with rather low resolutions of 0.27–0.40 eV at the FWHM of the zero-loss peak to obtain sufficient intensity.

Figure 1(a) shows an electron microscope image of single-shell tubes. The many winding fibers seen are bundles of single-shell carbon nanotubes. Round dark particles around the bundles are nickel particles used as a catalyst, and many of them are covered with several layers of graphitic sheets. The black circle shows the 100 nm-diameter area from which electron energy-loss spectra were measured. Figure 1(b) is a high-resolution electron microscope image of the bundle of single-shell tubes indicated by the arrow in Fig. 1(a). The single-shell tube is 1.0–1.3 nm in diameter.[6)]

Figure 2 shows an electron energy-loss spectrum in an energy region from 0 to 45 eV obtained from the bun-

*Present address: Central Research Laboratory, Sumitomo Metal Mining Co., Ltd., 3-18-5 Nakakokubun, Ichikawa 272.

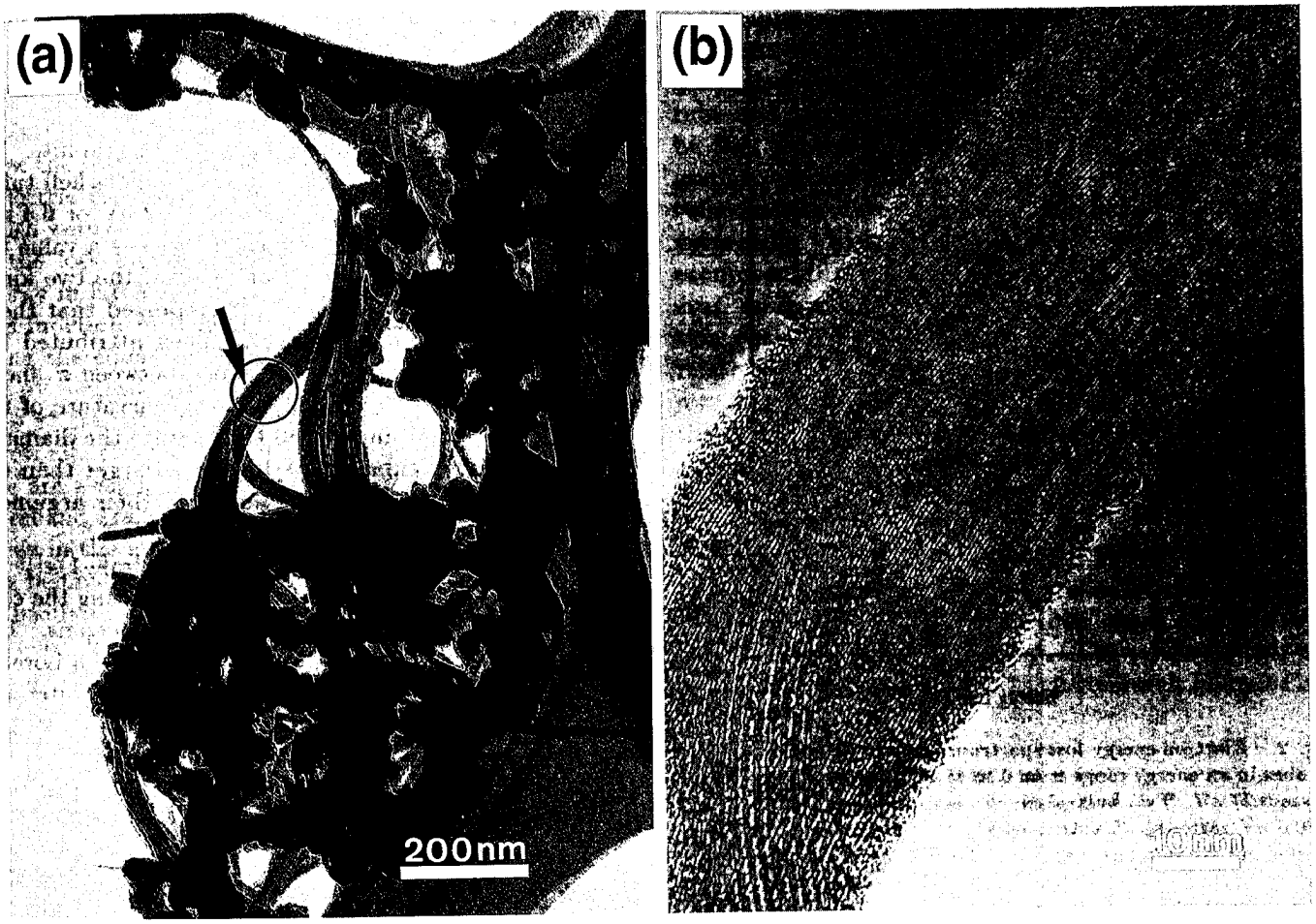

Fig. 1. (a) Electron microscope image of bundles of single-shell tubes. The black circle indicates the area from which electron energy-loss spectra were measured. The diameter of the circle is 100 nm. (b) High-resolution electron microscope image of the bundles of the single-shell tubes indicated by the arrow in (a).

dle of single-shell tubes indicated by the black circle in Fig. 1(a). The energy resolution was 0.27 eV for the FWHM of the zero-loss peak. Electron energy-loss spectra of graphite and of a multishell tube of 31 nm diameter with 44 graphitic sheets are also shown for comparison. Two prominent peaks indicated by arrows can be seen at 5.8 eV and 20.6 eV. The large peak at 20.6 eV is assigned to the collective excitation of all the valence electrons ($\pi + \sigma$ plasmon). The energy of the $\pi + \sigma$ plasmon peak is lower than those of the multishell tube and graphite. As mentioned in our previous work on multishell tubes,[13] the value of the $\pi + \sigma$ plasmon energy was determined as the mean value of the plasmon energies measured with electron incidences parallel and perpendicular to the c-axis of graphite. The value of the $\pi + \sigma$ plasmon energy of the single-shell tubes can be interpreted as follows. Electron diffraction patterns obtained from the bundle of single-shell tubes exhibit several diffraction spots which show the tubes to be packed hexagonally. Saito *et al.*[6] observed a cross section of a close-packed bundle of single-shell tubes in a high-resolution electron microscope image. Figure 3 shows a schematic diagram of the hexagonally packed bundle. The density N of carbon atoms of the bundle is given by

$$N = \frac{16\pi r}{3a^2(2r+d)^2} \tag{1}$$

from a geometrical calculation, where r is the radius of the single-shell tube, a is the lattice constant in the graphitic sheet and d is the distance between two neighboring single-shell tubes. The plasmon energy $\hbar\omega_p$ due to four valence electrons (one π electron and three σ electrons) is calculated using the equation

$$\hbar\omega_p = \hbar\sqrt{\frac{4Ne^2}{m\epsilon_0}}, \tag{2}$$

where ϵ_0 is the dielectric permittivity of vacuum, e is the electron charge, and m is the rest mass of an electron. By using the average diameter of the single-shell tubes observed, $2r = 1.15$ nm, and assuming $a = 0.246$ nm (the lattice constant of graphite) and $d = 0.34$ nm (the distance between the graphitic sheets in graphite), the $\pi + \sigma$ plasmon energy is calculated to be 19.9 eV, which shows good agreement with the experimental value. The plasmon peak energy is shifted to a higher energy than the calculated one by the interaction with the interband transition at about 11eV between σ and σ^* electron energy states (as seen in the ϵ_2 curve of Fig. 4). However, a relatively large damping factor or a wide width of about 11 eV of the plasmon peak causes a shift to a lower energy. Both effects almost cancel out the energy shift of the plasmon peak. As a result, the calculated energy of the plasmon peak based on a simple theory shows

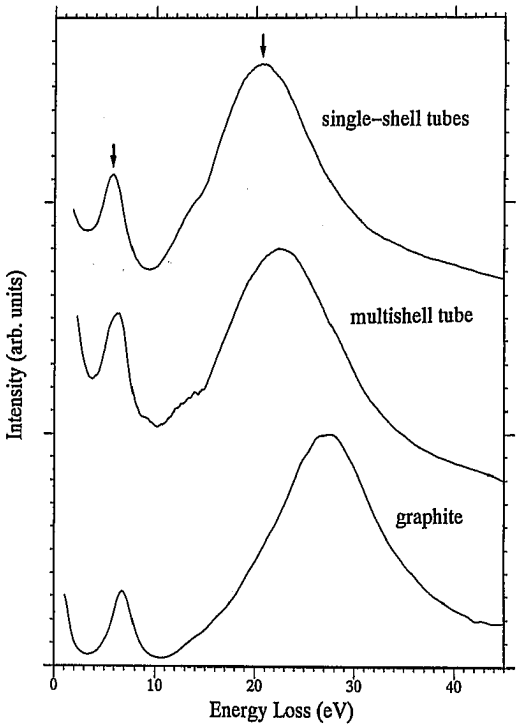

Fig. 2. Electron energy-loss spectrum of the bundle of single-shell tubes in an energy range from 0 to 45 eV. The energy resolution was 0.27 eV. Two bulk plasmon peaks are seen at 5.8 eV and 20.6 eV (arrows). Electron energy-loss spectra of a multishell tube and graphite are also shown for comparison.

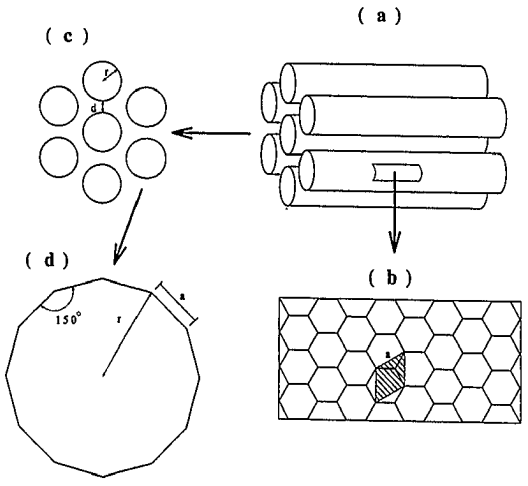

Fig. 3. (a) Schematic diagram of a bundle of single-shell tubes. It is assumed that single-shell tubes are packed hexagonally. (b) Graphitic sheet of an atomic-layer wall of the single-shell tube. a is the lattice constant. (c) Cross section of the bundle. r is the radius of the single-shell tube and d is the distance between the two neighboring single-atomic-layer walls.

good agreement with the experimental one. The energy of the $\pi + \sigma$ plasmon was different for multishell tubes with different diameters. In contrast, electron energy-loss spectra measured from four bundles of single-shell tubes showed the same plasmon energy. This can be interpreted by the fact that every graphitic sheet of the single-shell tube in the bundle has the same curvature, while the mean curvature of the graphitic sheets in multishell tubes are different for tubes with different diameters.

The peak at 5.8 eV is assigned to the π plasmon caused by an interband transition between π and π^* electron energy states by referring to the result of graphite. We reported[13] that there are two kinds of multishell tubes which exhibit the π plasmon peak at 5.2 eV or 6.4 eV. The energy of 5.8 eV of single-shell tubes is a value between those of the π plasmon energies of the two kinds of multishell tubes. Wang *et al.*[15] reported that the π plasmon peak was not observed. They attributed the absence of the peak to the difference between π and σ electrons being lost due to the strong curvature of the graphitic sheet in a single-shell tube. Since the diameter of the single-shell tube of 1.0–1.3 nm is larger than the diameter (0.71 nm) of a C_{60} cluster,[20] their argument may be incorrect.

Figure 4(a) shows the loss function ($\mathrm{Im}[-1/\epsilon]$) obtained from the spectrum of Fig. 2 by removing the contributions due to multiple scattering of electrons. The intensity of the direct beam was subtracted by a Lorentz fit. The absolute value of the loss function is often determined by the condition $\mathrm{Re}[-1/\epsilon(0)] \simeq -1/\epsilon_1(0) = -1/n^2$, where n is the refractive index. However, since the value of the refractive index of the single-shell tube is not known, the sum rule[21]

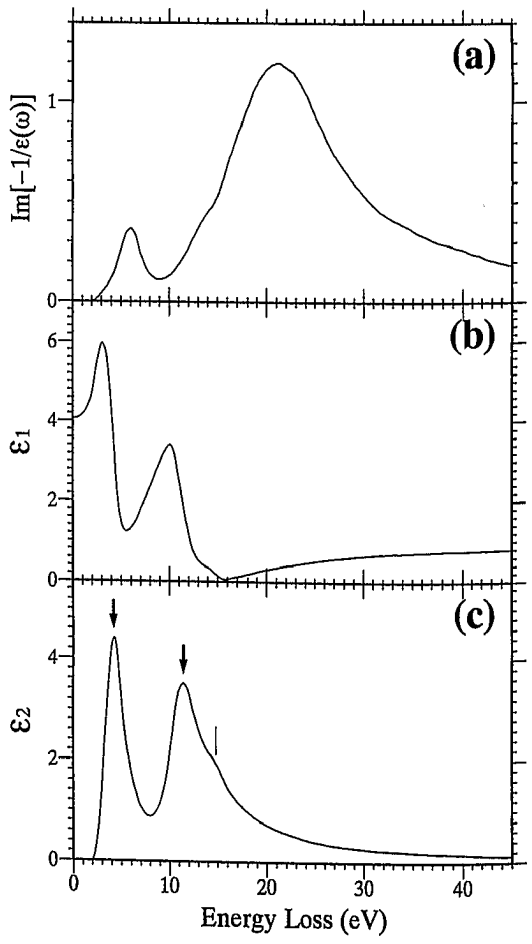

Fig. 4. The loss function (a), the real part (b) and the imaginary part (c) of the dielectric function of the bundle of single-shell tubes. The dielectric functions were obtained by Kramers-Kronig analysis of the loss function.

$$\int_0^\infty \omega \mathrm{Im}[-1/\epsilon(\omega)]\mathrm{d}\omega = \frac{\pi}{2}{\omega_\mathrm{p}}^2 \qquad (3)$$

is used to determine the absolute value. The value of $\hbar\omega_\mathrm{p}$ is taken to be 19.9 eV from eq. (2). Figures 4(b) and 4(c) show the real part (ϵ_1) and the imaginary part (ϵ_2) of the dielectric function of the single-shell tubes,respectively, which were obtained by Kramers-Kronig analysis (KKA) of the loss function. The integration with respect to energy in KKA was carried out up to 400 eV, where the loss function in a high-energy region was extrapolated using the equation AE^{-b}, where $b = 4.0$. The peak at 4.2 eV indicated by an arrow in ϵ_2 is assigned to the $\pi \rightarrow \pi^*$ transition. The peak at 11.4 eV indicated by an arrow and the shoulder at 14.9 eV indicated by a vertical line are assigned to the $\sigma \rightarrow \sigma^*$, $\sigma \rightarrow \pi^*$ and $\pi \rightarrow \sigma^*$ interband transitions. The ϵ_2 curve of the single-shell tubes in the low-energy region (0–2 eV) shows insulator like behavior. However, whether the single-shell tube is an insulator or not cannot be determined from the curve, because the ϵ_2 in a region from 0 to 2 eV is not accurate enough owing to errors introduced by the subtraction of zero-loss intensity from the raw data by a Lorentz fit.

Figure 5 shows carbon K-absorption edge spectra of the bundle of single-shell tubes, the multishell tube and graphite. The energy resolution was 0.40 eV for the FWHM of the zero-loss peak. Transitions from 1s to the unoccupied π^* levels are seen at 286eV and those to the unoccupied σ^* levels are seen to begin at about 292 eV in the three spectra. We have mentioned in our previous EELS work on multishell tubes[13] that the 1s$\rightarrow \pi^*$ transition peak of the multishell tube is slightly broader than that of graphite. This was explained by the broadening of the π^* energy states due to the curvature of the graphitic sheets. Not only the 1s$\rightarrow \pi^*$ transition peak but also the 1s$\rightarrow \sigma^*$ transition peak of the single-shell tubes are much broader than those of the multishell tube and graphite. The reason for the broadening may be that a bundle of single-shell tubes consists of only graphitic sheets with a small radius, while the multishell tube consists of many graphitic sheets with different curvatures, in which the graphitic sheets with larger radii occupy a greater part of the volume. There is, however, an experiment[22] proving that the 1s$\rightarrow \pi^*$ transition peak measured from one single-shell tube shows a relatively sharp peak similar to that of graphite. In such a case, the broadening of the 1s$\rightarrow \pi^*$ transition peak in the present study may be not due to the strong curvature of the graphitic sheet but due to the effect of bundle formation.

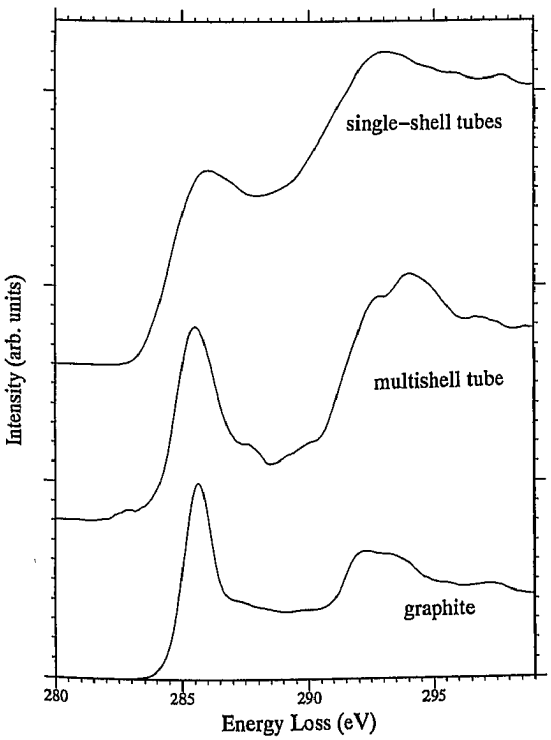

Fig. 5. Carbon K-absorption edge spectra of the bundle of single-shell tubes, multishell tube and graphite. The energy resolution was 0.40 eV.

Acknowledgement

The authors thank Mr. Y. Harada, Dr. K. Tsuno and Mr. J. Ohyama of JEOL for their great effort in constructing the EELS instrument. The present work was partly supported by the KAZATO Research Foundation.

1) S. Iijima: Nature **354** (1991) 56.
2) X. K. Wang, X. W. Lin, V. P. Dravid, J. B. Ketterson and R. P. H. Chang: Appl. Phys. Lett. **62** (1993) 1881.
3) S. Iijima and T. Ichihashi: Nature **363** (1993) 603.
4) D. S. Bethune, C. H. Kiang, M. S. deVries, G. Gorman, R. Savoy, J. Vazquez and R. Beyers: Nature **363** (1993) 605.
5) Y. Saito, T. Yoshikawa, M. Okuda and N. Fujimoto: to be published in J. Phys. Chem. Solids.
6) Y. Saito, M. Okuda, N. Fujimoto, T. Yoshikawa, M. Tomita and T. Hayashi: Jpn. J. Appl. Phys. **33** (1994) L526.
7) N. Hamada, S. Sawada and A. Oshiyama : Phys. Rev. Lett. **68** (1992) 1579.
8) R. Saito, M. Fujita, G. Dresselhaus and M. S. Dresselhaus: Phys. Rev. B **46** (1992) 1804.
9) R. Saito, M. Fujita, G. Dresselhaus and M. S. Dresselhaus: Appl. Phys. Lett. **60** (1992) 2204.
10) M. S. Dresselhaus, G. Dresselhaus and R. Saito: Phys. Rev. B **45** (1992) 6234.
11) J. W. Mintmire, B. I. Dunlap and C. T. White: Phys. Rev. Lett. **68** (1992) 631.
12) K. Tanaka, K. Okahara, M. Okada and T. Yamabe: Chem. Phys. Lett. **191** (1992) 469.
13) R. Kuzuo, M. Terauchi and M. Tanaka: Jpn. J. Appl. Phys. **31** (1992) L1484.
14) V. P. Dravid, X. Lin, Y. Wang, X. K. Wang, A. Yee, J. B. Ketterson and R. P. H. Chang: Science **259** (1993) 1601.
15) X. K. Wang, X. W. Lin, V. P. Dravid, S. N. Song, J. B. Ketterson and R. P. H. Chang: *Proc. 2nd Int. American Congress on Electron Microscopy* (Cancun, Mexico, 1993).
16) K. Tsuno, M. Terauchi and M. Tanaka: Optik **83** (1988) 77.
17) M. Terauchi, R. Kuzuo, F. Satou, M. Tanaka, K. Tsuno and J. Ohyama: *Proc. Int. Congress for Electron Microscopy* (San Francisco Press, San Francisco, 1990).
18) M. Terauchi, R. Kuzuo, F. Satou, M. Tanaka, K. Tsuno and J. Ohyama: Microsc. Microanal. Microstruct. **2** (1991) 351.
19) M. Kato and K. Tsuno: Nucl. Instrum. & Methods in Phys. Res. **A298** (1990) 296.
20) Y. Saito, T. Yoshikawa, N. Fujimoto and H. Shinohara: Phys. Rev. B **48** (1993) 9182.
21) H. Raether: *Excitation of Plasmons & Interband Transitions by Electrons* (Springer, Berlin, Heidelberg, New York, 1980) Springer Tract in Modern Physics Vol. 88.
22) C. Colliex: private communication.